

# THE SIMULATION STUDY ON LAND SURFACE ENERGY BUDGET OVER CHINA AREA BASED ON LIS-NOAH LAND SURFACE MODEL

CHEN Yingying<sup>ab</sup>, SHI Jiancheng<sup>a</sup>, QI Yuanyuan<sup>ab</sup>, JIANG Lingmei<sup>c</sup>

<sup>a</sup> State Key Laboratory of Remote Sensing Science, Institute of Remote Sensing Applications, CAS, Beijing 100101, ldgen@126.com

<sup>b</sup> Graduate school of Chinese Academy of Sciences, Beijing 100049, ldgen@irsa.ac.cn

<sup>c</sup> School of Geography, Beijing Normal University, Beijing 100875, jlinmei@263.net

## Commission VIII, WG VIII/3

**KEY WORDS:** Land Information system, Noah Land Surface Model, Simulation, Surface Energy Balance

### ABSTRACT:

The availability of time series of water and land surface energy budgets over China area is essential for understanding the environmental system and potential climate change in this area. However, consistent observations of the land surface state variables are routinely unavailable. In the absence of long-term observations of the components of the water and land surface energy budgets, modeling can provide consistent fields of land surface fluxes and states. We simulated the components of surface energy balance (SEB) equation using Land Information System (LIS) for time period of 2002.11-2003.12. Residual analyses of SEB indicate that the distribution of residuals show some spatial and temporal characteristics. The temporal characteristics of residual distribution suggest that LIS can simulate energy flux better in spring and summer than in other time. The spatial characteristics indicate that LIS can simulate energy flux better in places with relative low latitude or low altitude than in places with either higher latitude or higher altitude. This kind of temporal and special distribution pattern probably related to the parameterization of snow albedo. The results of comparison between simulated and MODIS land surface temperature(LST) indicate that mostly difference between two LST are within  $\pm 5K$ . The scatter plots and standard deviation suggests that the simulated LST of night\_view\_time is 2-3K accurate than that of day\_view\_time.

### 1. INTRODUCTION

The availability of time series of water and land surface energy budgets over China area is essential for understanding the environmental system and potential climate change in this area. However, consistent observations of components of the land surface water and energy budgets are routinely unavailable over large scales (Sheffield et al. 2006). Otherwise, the heterogeneity in topography, soil, and vegetation characteristics further complicates the difficulty with interpretation of the traditional "point" measurement on the local scale and the

understanding of its dynamics (Fei Chen et al. 2004). On the other hand, increasingly improving remote sensing techniques hold the promise of monitoring the surface soil moisture and surface energy budgets at high resolution over a large domain up to global scale, but remote sensing is restricted to indirect quantities, in the case of soil moisture, to low-vegetated regions and the top few centimeters. Another way to estimate large-scale water and energy cycle terms is to use land surface models, in either offline or coupled modes (e.g., Lau et al. 1994; Liang et al. 1994; Levis et al. 1996; Werth and Avissar 2002). Land surface model close the water and energy budget by

construct, so if the meteorological forcing data are accurate and model biases are small, these constructed water and energy balance terms might be used in lieu of observations and provide a consistent picture of the water and energy budgets (Sheffield et al. 2006). Unfortunately, it is hard to completely remove errors in forcing data and model biases. So with these state variables being integrated forward the errors in land surface forcing and parameterization are accumulated, which leads to incorrect surface water and energy partitioning. Results from the North America Land Data Assimilation System project (K. E. Mitchell et al. 2004) indicated that first-order errors in the land surface simulations were due to inaccurate specification of the forcings and especially in precipitation (Robock et al. 2003; Pan et al. 2003). Actually, analyses of water and energy cycle variables estimated through observations (in situ and/or remote sensing) will not provide water cycle closure (Roads et al. 2003; Pan and Wood 2004) because of sampling and retrieval errors.

However, many innovative new land surface observations are becoming available that may provide additional information necessary to constrain the initialization of land surface states critical for long-term prediction. These constraints can be imposed in two ways. Firstly, by forcing the land surface primarily by observations (such as precipitation and radiation), the often severe atmospheric numerical weather prediction land surface forcing biases can be avoided. Secondly, by employing innovative land surface data assimilation techniques, observations of land surface storages can be used to constrain unrealistic simulated storages (Paul R. Houser et al. 2000). Global Land Data Assimilation System, which is developed jointly by scientists at the National Aeronautics and Space Administration (NASA) Goddard Space Flight Center (GSFC) and the National Oceanic and Atmospheric Administration (NOAA) National Centers for Environmental Prediction (NCEP) (M. Rodell, 2004), is a high-resolution, near-real-time land data assimilation scheme using relevant remotely-sensed and in-situ observations within a land data assimilation framework.

In this study we used Land Information System, which is the software platform of GLDAS, to simulate the components of land surface energy budget over China area, and test the internal consistency of LIS using residual analyses method. We also compared simulated land surface temperature with the Moderate Resolution Imaging Spectroradiometer Aqua Land

Surface Temperature/Emissivity Daily L3 Global 0.05Deg CMG data over this area.

## 2. STATE VARIABLES SIMULATION

LIS core can invoke several community land surface models such as CLM (Dai et al. 2003), and Noah (Chen et al. 1996; Koren et al. 1999). In this study we use Noah land surface model to simulate the surface state variables. The Noah land surface model was developed by the US National Centers for Environment Prediction and other investigators from both public and private institutions under the framework of the Global and Energy Water Cycle Experiment (GEWEX) Continental-Scale International Project (GCIP).

### 2.1 Input Data

The input data to Noah land surface model include following data sets:

**Forcing data:** in this study we use the Global Data Assimilation System (*GLDAS*), which is the operational global atmospheric data assimilation system of NCEP (Derber et al. 1991), to provide near-surface air temperature, near-surface specific humidity, near-surface wind field, surface pressure, downward shortwave radiation, and downward longwave radiation. The precipitation is provided by observation-derived National Oceanic and Atmospheric Administration (NOAA) Climate Prediction Center's (CPC's) operational global 2.5° 5-day Merged Analysis of Precipitation (*CMAP*), which is a blending of satellite and gauge observations. GDAS modeled precipitation fields are used to disaggregate the CMAP fields spatially and temporally to match the GLDAS resolutions.

**Land surface parameter. Vegetation:** In this simulation, we use a static, 1-km resolution, global dataset of land cover class that was produced at the University of Maryland (UMD) based on observations from the Advanced Very High Resolution Radiometer (AVHRR) aboard the NOAA-15 satellite (Hansen et al. 2000). We also employ monthly greenness fraction climatology data (G. Gutman et al. 1998), which is derived from NOAA/AVHRR normalized difference vegetation index (NDVI) data, as an input to evapotranspiration schemes in Noah model. **Soil:** The soil parameter data used in this study were derived from the 5' resolution soil map of the world,

global soil profile databases (Reynolds et al. 2000). Porosity and the percentages of sand, silt, and clay were horizontally resampled to 0.25° grid and vertically interpolated to 0-2-, 2-150-, 150-350-cm depths. **Elevation:** The global 30-arc-s GTOPO30 were averaged onto 0.25° grid, and are used to corrects the modeled temperature, pressure, humidity, and longwave radiation forcing fields based on the difference between the LIS elevation definition and the elevation definition of the model that created the forcing data, following Cosgrove et al.(2003). **The other parameter datasets** include Quarterly albedo climatology using as surface albedo fraction (snow-free), Maximum snow albedo, bottom temperature serves as the annually fixed soil-temperature bottom-boundary condition, Noah soil look-up table, and UMD land/sea mask.

## 2.2 Output Fields

The output variables of LIS are listed in tab.1. In this study we emphasized on the surface energy budgets, so the net shortwave radiation, net longwave radiation, latent heat flux, sensible heat flux, and ground heat flux are used to test consistency. The average surface temperature are selected to compare with MODIS MYD11C1 0.05Deg. CMG land surface temperature data.

Table 1. LIS output fields

Output fields	unit
Latent, sensible, and ground heat flux	W/m <sup>2</sup>
Net surface shortwave and longwave radiation	W/m <sup>2</sup>
Soil moisture of 4 layers, RootMoist	kg/m <sup>2</sup>
Soil Wetness	-
Soil temperature of 4 layers, Average surface temperature	K
Snowfall and rainfall	kg/m <sup>2</sup> /s
Snow water equivalent	kg/m <sup>2</sup>
Change of soil moisture, Change of snow water equivalent	kg/m <sup>2</sup>
Surface and subsurface runoff	kg/m <sup>2</sup> /s
Snowmelt	kg/m <sup>2</sup> /s
Vegetation transpiration, Bare soil evaporation, Total Evapotranspiration	kg/m <sup>2</sup> /s
Albedo	-

## 2.3 Study Area and Time Period

The *study area* was chosen as northeast part of Asian

(15.75-56°N, 70.75-138°), mainly in China area. The simulation *time period* is from 2002.11.01 to 2003.12.01. The *spatial resolution* is 0.25°×0.25°, and the *temporal resolution* is 3-hourly (UTC 00, 03, 06, 09, 12, 15, 18, 21).

## 3. RESIDUAL ANALYSIS AND COMPARISON OF LAND SURFACE TEMPERATURE

### 3.1 Residual Analysis of Simulated Energy Budget

As required in the PILPS experiments for phase 2a (Chen et al. 1997), outputs from a land surface scheme should first be checked to ensure the conservation of energy and water. This requirement is absolutely necessary since it is extremely difficult, if not impossible, to know whether or not a scheme's algorithms are valid. The surface energy balance (SEB) equation can be given as

$$\begin{aligned} R_{net} &= SW_{net} + LW_{net} = (1-\alpha)S_{\downarrow} + \epsilon L_{\downarrow} - \epsilon\sigma T_{sfc}^4 \\ &= Q_{le} + Q_h + Q_g \end{aligned} \quad (1)$$

Where the coefficient  $\alpha$  in (1) is the surface albedo,  $\sigma$  is the Stefan-Boltzmann constant, and  $\epsilon$  is the ground surface emissivity. The  $R_{net}$  is the net radiation, which is consist of net shortwave radiation and net longwave radiation.  $S_{\downarrow}$ ,  $L_{\downarrow}$  and  $T_{sfc}$  are incoming shortwave radiation, incoming longwave radiation and ground surface temperature respectively. On the right-hand side of (1),  $Q_{le}$  and  $Q_h$  are the latent and sensible heat fluxes, respectively. The term  $Q_g$  is the soil heat flux at the surface. We calculated the quarterly averages of the components in the SEB equation from simulated data, and analyzed the residual of SEB equation, with the residual defined as the difference between the left- and the right-hand sides of the equation, which can be written as

$$Residual = R_{net} - (Q_{le} + Q_h + Q_g) \quad (2).$$

Figure 1 shows the spatial distribution of quarterly residual of SEB equation and it's histogram in study area in 2003. We make a statistic of the residuals of 33720 grids (excluding 9589 grids for water body). It indicates that the distribution of residuals show some spatial and temporal characteristics. The percentage of grids with absolute value of residual less than 3 W/m<sup>2</sup> are 94.42%, 95.64%, 96.9%, and 68.61% in winter(DJF),

spring(MAM), summer (JJA) and autumn(SON) ,respectively. The percentage of grids with absolute value large than 10 W/m<sup>2</sup> are 2.99%, 0.31%, 0.43%, 3.97% in winter, spring, summer and autumn, respectively. And the percentage of grids whose absolute value large than 3 W/m<sup>2</sup> and less than 10 W/m<sup>2</sup> are 2.59%, 4.03%, 2.67%, and 27.42% in winter, spring, summer and autumn, respectively. Those grids mainly distribute in south and middle part of Qinghai-Tibet plateau and in North-East part of China, including Heilongjiang, part of Jilin and Liaoning province, and east part of inner Mongolia. The geo-distribution of residual for yearly average has the same spacial pattern(not show ).

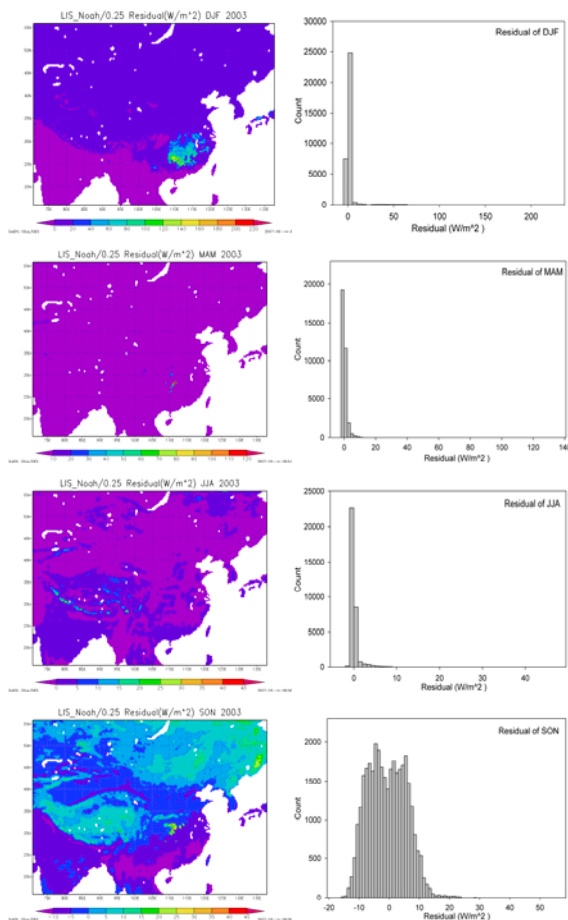


Figure 1. Spatial distribution of Quarterly residual of SEB equation and its histogram over China area, 2003

The temporal characteristics of residual distribution suggest that LIS can simulate energy flux better in spring and summer than in autumn and winter. The spacial characteristics of residual distribution indicate that LIS can simulate energy flux better in places with relative low latitude or low altitude than in Qinghai-Tibet plateau and North-East part of China, which has either higher latitude or higher altitude. The temporal and

special distribution pattern of residual most probably related to the parameterization of snow albedo in LIS-Noah land surface model. It is obviously known that snow have great effects on land surface energy balance, because it can greatly changes the albedo of land surface. In autumn and winter the snow occur and it is easier remained in relative high latitude and high altitude areas in China. In LIS-Noah model the snow albedo is calculated based on the snow cover, Quarterly albedo climatology and Maximum snow albedo datasets. It is supposed that directly using the MODIS-derived albedo data is better.

### 3.2 The Comparison of Land Surface Temperature Between Simulated and MODIS

We compared the simulated Noah land surface temperature(LST) with MODIS MYD11C1 land surface temperature/emissivity daily L3 global 0.05deg CMG product. This product contains day\_view LST and night\_view LST . Because this product is usually contaminated by cloud, we make a statistic of the grid with valid value (means there were no cloud over this grid when the satellite passed by) of every day's data from 2003.01.01 to 2003.12.01. We selected one day\_view LST product whose cloud coverage is least in each uneven month and one night\_view LST product whose cloud coverage is least in each even month to be used in calibration the simulated LST. These days are 2003.01.20, 2003.02.06, 2003.03.23, 2003.04.06, 2003.05.01, 2003.06.02, 2003.07.17, 2003.08.24, 2003.09.22, 2003.10.22, and 2003.11.17.

In order to compare the LST in same spacial scale in 0.25°, we preprocessed the MYD11C1 product and the simulated LST by following strategies: (1) we aggregated the selected MYD11C1 LST to 0.25°spacial resolution, the upscaling strategy is in every 25 0.05° grids if there are more than 18 grids have valid LST then we use the average of these grids as the value of the aggregated grid so that the cloud coverage of this grid is less than 28%. The percentage of area for places with cloud coverage less than 28% in study area for selected days mentioned above are 44.6%, 58.6%, 47.4%, 49.3%, 54.1%, 51.7%, 43.1%, 43.9%, 50.8%, 45.9%, 51.4%, respectively. Those who don't satisfy the aggregated condition, we set their values as undefined values. (2) Each MYD11C1 grid has it's own view time, and these view time are different, so we aggregated the corresponding view time of each selected MYD11C1 product using the same strategy in (1), then we

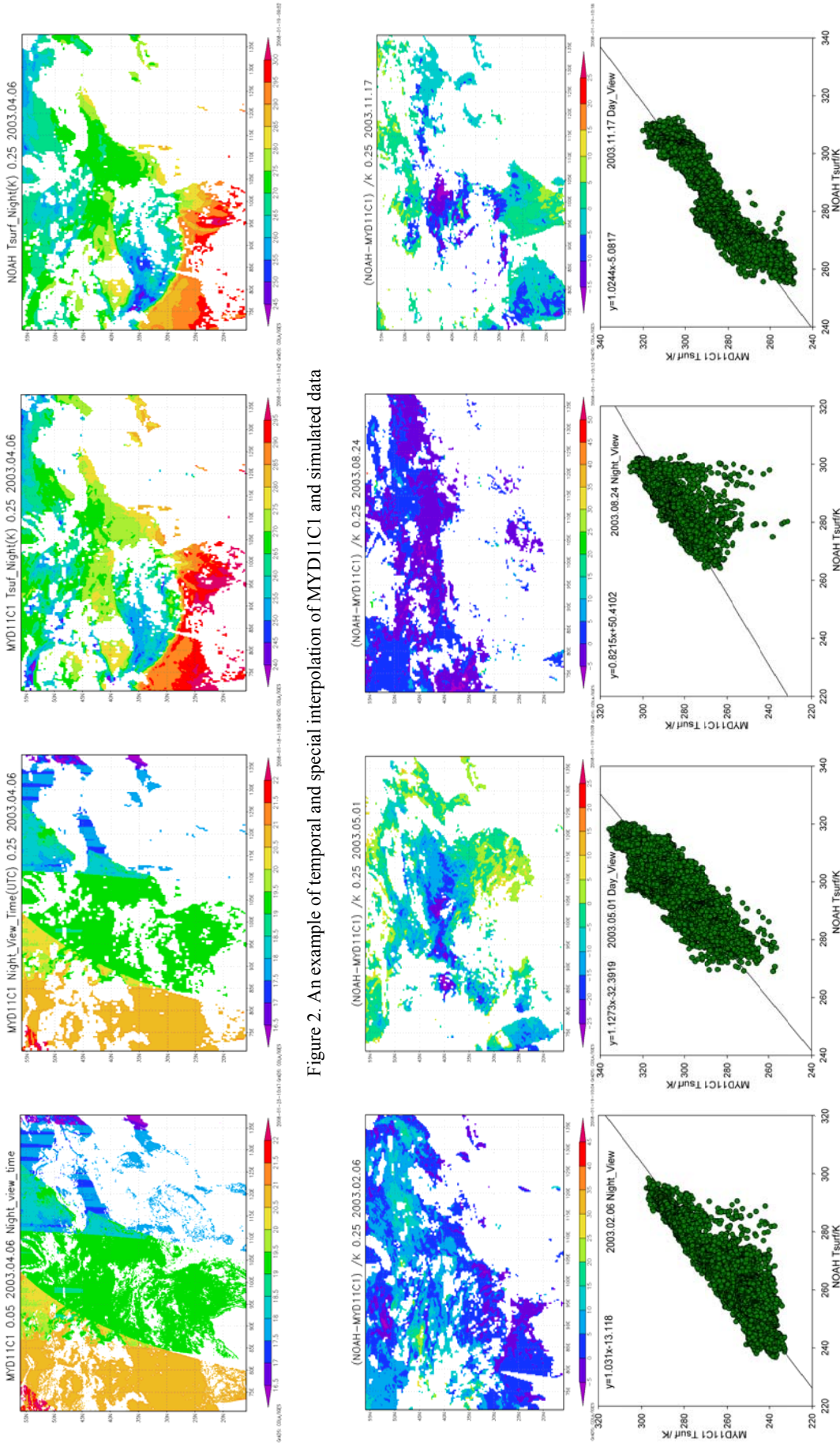


Figure 2. An example of temporal and special interpolation of MYD11C1 and simulated data

Figure 3. The comparison of Noah LST with aggregated MYD11C1 LST. The top column shows the spatial distribution of difference between simulated Noah LST and MYD11C1 LST for 2003.02.06, 2003.05.01, 2003.08.24, 2003.11.17. The bottom column shows the corresponding scatter plots of the two LST

interpolated the simulated Noah LST to the aggregated MYD11C1 LST in temporal and matched the simulated data with the 0.25° MYD11C1 data. Figure 2 shows the temporal and special interpolated MYD11C1 and simulated data of 2003.04.06 as an example, the first panel is the original MYD11C1 night\_view\_time, the second panel is spatial interpolated MYD11C1 night\_view\_time, the third panel is the spatial interpolated MYD11C1 LST, and the fourth panel is the temporal interpolated and special matched simulated Noah LST. As to the spatial interpolation strategy, because using the averaged value as the aggregated grid value, the errors of aggregated LST are reduced than original ones. So the aggregated MYD11C1 LST can objectively represent the LST of 0.25° grids. As to the temporal interpolation strategy, the temporal resolution of simulated LST are 3-hourly, the result is interpolated from adjacent two simulated Noah LST.

Figure 3 shows the spatial distribution of difference between simulated Noah LST and MYD11C1 LST, and the corresponding scatter plot of the two LST for selected days. Those plots show that the simulated Noah LST and the aggregated MYD11C1 LST have very similar spatial distribution pattern and the differences between them are mostly within ±5K. There are also few differences whose absolute values are larger than 5K, which sparsely distributed in study area without explicit spatial pattern.

Table 2. The statistic characteristics of the simulated surface temperature with MYD11C1 LST.

Date	y=ax+b		Correla -tions	Std Dev (K)
	a	b		
03.01.20	1.033	-5.520	0.915	8.133
03.03.23	0.893	35.598	0.833	9.744
D 03.05.01	1.127	-32.392	0.835	8.840
a 03.07.17	0.913	29.138	0.666	7.904
y 03.09.22	0.803	62.309	0.687	8.224
03.11.17	1.024	-5.082	0.947	5.601
N 03.02.06	1.031	-13.118	0.932	7.069
i 03.04.06	1.058	-18.579	0.914	6.045
g 03.06.02	0.991	2.093	0.888	4.125
h 03.08.24	0.822	50.410	0.793	4.210
t 03.10.22	1.025	-8.007	0.924	4.468

Note: x represent Noah simulated surface temperature, y represent the MYD11C1 surface temperature.

Table 2 gives some statistic characteristics of the simulated

surface temperature with MYD11C1 LST. In general, the correlation coefficient of simulated day\_view LST is greater than that of simulated night\_view LST. The standard deviation between two LST explicitly indicate that the simulated night\_view LST is 2-3K accurate than the simulated day\_view LST.

#### 4. CONCLUSIONS

Land Information System is developed to be used in studying and simulating the water and energy budget occurred in land surface. In this study we use LIS to simulate the components of surface energy budget equation, the results of consistency test and comparison of simulated LST with MYD11C1 LST suggest that LIS is a proper choice to study surface energy budget issues.

#### REFERENCE

- Chen, F., and Coauthors, 1996: Modeling of land-surface evaporation by four schemes and comparison with FIFE observations. *J. Geophys. Res.*, 101 (D3), 7251–7268.
- Chen F., Kevin W., David N. et al., 2004: Development of High Resolution Land Data Assimilation System and its Application to WRF, AMS 16th Conference on Numerical Weather Prediction. 11-15 January 2004, Seattle, WA.
- Chen, T. H., and Coauthors, 1997: Cabauw experimental results from the Project for Intercomparison of Land-Surface Parameterization Schemes. *J. Climate*, 10, 1194–1215.
- Cosgrove, B. A., and Coauthors, 2003: Real-time and retrospective forcing in the North American Land Data Assimilation System (NLDAS) project. *J. Geophys. Res.*, 108, 8842, doi:10.1029/2002JD003118.
- Dai Y., and Coauthors, 2003: The Common Land Model (CLM). *Bull. Amer. Meteor. Soc.*, 84, 1013–1023.
- Derber, J. C., D. F. Parrish, and S. J. Lord, 1991: The new global operational analysis system at the National Meteorological Center. *Wea. Forecasting*, 6, 538–547.

- Gutman, G., and A. Ignatov (1998), The derivation of the green vegetation fraction from NOAA/AVHRR data for use in numerical weather prediction models, *Int. J. Remote Sens.*, 19(8), 1533–1543.
- Hansen, M. C., R. S. DeFries, J. R. G. Townshend, and R. Sohlberg, 2000: Global land cover classification at 1km spatial resolution using a classification tree approach. *Int. J. Remote Sens.*, 21, 1331–1364.
- Houser P. R., Michael Bosilovich, Brian Cosgrove et al., 2000: A Global Land Data Assimilation Scheme (GLDAS), Proposal Submitted to NRA-99-OES-04: NASA-ESE Modeling and Data Analysis Research, EOS/IDS
- Koren, V., J. Schaake, K. Mitchell, Q. Y. Duan, F. Chen, and J. M. Baker, 1999: A parameterization of snowpack and frozen ground intended for NCEP weather and climate models. *J. Geophys. Res.*, 104, 19 569– 19 585.
- Lau, K.-M., V. M. Mehta, Y. C. Sud, and G. K. Walker, 1994: Climatology and natural variability of the global hydrologic cycle in the GLA atmospheric general circulation model. *J. Geophys. Res.*, 99 (D1), 1329–1345.
- Levis, S., M. T. Coe, and J. A. Foley, 1996: Hydrologic budget of a land surface model: A global application. *J. Geophys. Res.*, 101 (D12), 16 921–16 930.
- Liang, X., D. P. Lettenmaier, E. F. Wood, and S. J. Burges, 1994: A simple hydrologically based model of land surface water and energy fluxes for general circulation models. *J. Geophys. Res.*, 99 (D7), 14 415–14 428.
- Mitchell, K. E., and Coauthors, 2004: The multi-institution North American Land Data Assimilation System (NLDAS) project: Utilizing multiple GCIP products and partners in a continental distributed hydrological modeling system. *J. Geophys. Res.*, 109, D07S90, doi:10.1029/2003JD003823.
- Reynolds, C. A., T. J. Jackson, and W. J. Rawls, 2000: Estimating soil water-holding capacities by linking the Food and Agriculture Organization soil map of the world with global pedon databases and continuous pedotransfer functions. *Water Resour. Res.*, 36, 3653– 3662.
- Robock, A., and Coauthors, 2003: Evaluation of the North American Land Data Assimilation System over the Southern Great Plains during the warm season. *J. Geophys. Res.*, 108, 8846, doi:10.1029/2002JD003245.
- Rodell M., Houser P. R., Jambor U. et al., 2004: The Global Land Data Assimilation System, *Bulletin of the American Meteorological Society*, 85(3), 381–394
- Sheffield, J., G. Goteti, and E. F. Wood, 2006: Development of a 50-yr high-resolution global dataset of meteorological forcings for land surface modeling, *J. Climate*, 19 (13), 3088-3111.
- Pan, M., and E. F. Wood, 2004: Water budget estimation by assimilating multiple observations and hydrological modeling using constrained ensemble kalman filtering. *Eos, Trans. Amer. Geophys. Union*, 85 (Suppl.).
- Werth, D., and R. Avissar, 2002: The local and global effects of Amazon deforestation. *J. Geophys. Res.*, 107, 8087, doi:10.1029/2001JD000717.

